Mathematical Modeling of the Flow of Diesel-CNG Fuel Mixture in a Pipe under the Influence of a Magnetic Field

H. A. Abdul Wahhab[†], A. R. A. Aziz, H. H. Al-Kayiem and M. S. Nasif

Mechanical Engineering Department, Universiti Teknologi PETRONAS, Perak, Seri Iskandar, 32610, Malaysia

†*Corresponding Author Email: hasanain_g02853@utp.edu.my*

ABSTRACT

Horizontal bubbly flow is encountered in various gas and oil facilities and industrial systems. Bubbly flow is characterized by the ability to provide large interfacial areas for heat and mass transfer. Nonetheless, horizontal bubbly flow orientation has received less attention when compared to vertical bubbly flow. This paper presents development of mathematical model and discusses the results obtained from the simulation of hydro-magnetic flow of Diesel-CNG fuel mixture in a horizontal pipe, as predicted by the developed model. The fundamental equations of unsteady, two-phase liquid-gas under an imposed magnetic field were derived and presented. Derivation procedure of the velocity distribution of the liquid and gas phases and the inverse Stokes' number of a bubbly flow are presented. These governing nonlinear partial-differential equations have been solved numerically using a Fourier–Bessel series. Results obtained from the model solution show that the axial velocities of liquid and gas, in laminar flow, have decreased and the slip ratio has increased with the increase of the magnetic field intensity. While, the magnetic field parameter, Ha increased the probability of decreasing the bubbles radii and increasing the bubbles number $(n.R_b)$.

NOMENCLATURE

B	magnetic field intensity	u	axial velocity
E	electric field density	u_l	diesel axial velocity
F_{mag}	magnetic force	u_g	CNG axial velocity
F_{fric}	mutual friction force	$\bar{u}_l$	dimensionless Diesel axial velocity
G	pressure gradient	$\bar{u}_{\bar{g}}$	dimensionless CNG axial velocity
Ha	Hartmann number	σ	electric conductivity
J	current density	σ_o	electric conductivity of diesel
N	momentum transfer coefficient	α	void fraction
n	number of CNG bubbles	ρ_l	diesel density
r	radial distance	ρ_g	CNG density
$\bar{r}$	dimensionless radial distance	μ_l	diesel dynamic viscosity
R	pipe radius	μ_g	CNG dynamic viscosity
R_b	CNG bubble radius	β	inverse Stoke's number
s	density ratio	δ	viscosity ratio
t	time		

1. INTRODUCTION

In Diesel engines, the new idea of pre-mixing of Diesel fuel and CNG was suggested to increase the air quantity inside the cylinder more than if a mixture of CNG-air is injected in the engine,
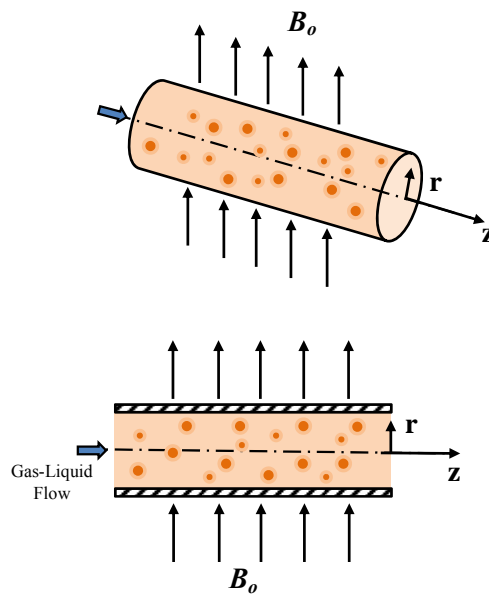
directly, which may result in a rich mixture, as reported by Abdul Wahhab *et al.* (2015). This pre-mixing technique requires a study of the behavior of the CNG gas bubbles in the Diesel liquid fuels. Also, the methods to control the bubbles sizes before arriving in the injection system through an

influence of external forces, such as a magnetic field, are essential to be understood. The horizontal bubbly flow pattern is characterized by the presence of bubbles dispersed in a continuous liquid phase, with their maximum size being much smaller than the diameter of the containing pipe. This particular flow orientation has received less attention when compared to vertical bubbly flow. Gedik *et al.* (2012) studied the unsteady viscous incompressible and electrically conducting of two phase fluid flow in circular pipes with external magnetic and electrical field. The influence of a magnetic field on the skin friction factor of steady fully-developed laminar flow through a pipe was studied experimentally by Malekzadeh *et al.* (2011), it was found that a transverse magnetic field changed the axial velocity profile from parabolic to a relatively flat shape, Chamkha and Ahmed (2011) explained that increasing the value of magnetic field parameter resulted in increment in the skin-friction coefficients while, the velocity components decreased with the increasing values of the magnetic parameter. Kumar *et al.* (2012) have solved the problem of steady, laminar flow and heat transfer of an electrically conducting fluid through vertical channel in the presence of uniform transverse magnetic field. He has formulated the problem mathematically using a two-fluid continuum model. They concluded that the increase in the Hartmann number works to suppress the flow velocity.

The problem of fully developed two fluid MHD flows with and without applied external forces such as electric field in an inclined channel have analyzed by Malashetty *et al.* (2000, 2001). In the same direction, Chang (1989) studied experimentally and numerically stratified gas-liquid two-phase electro-hydrodynamics in a pipe flow. He showed that the effect of the applied electric field is significantly influenced by the flow regime transition boundaries between the stratified smooth-to-wavy and stratified wavy-to-intermittent flow, and the time-averaged void fraction was not observed to be significantly influenced by the applied electric fields. Brunner *et al.* (1980) and Brunner *et al.* (1983) suggested that the flow pattern may be controlled by electro-hydrodynamic forces, and several flow pattern transition mechanisms were presented. The analysis of a liquid-gas flow begins with the most general principles governing the flow behavior namely; the conservation of mass, momentum, and energy. These principles can be expressed mathematically at every point in space and time by local, instantaneous field equations as reported by Attia (2003), Kumar and Prasad (2014), Chutia and Deka (2015). Some other researchers used computational simulation, using both, the volume-of-fluid method and level set method to analyze two phase flow, like Raessi *et al.* (2007). On other hand, Ghasemi *et al.* (2015) developed simulation procedure for system power output, vorticity flow field, and hydrodynamic coefficients. Mosayebidorcheh *et al.* (2015) solved the coupled flow and heat transfer equations and used a hybrid treatment base on finite difference method (FDM) and differential transform method (DTM).

In this work, a mathematical model has been developed and solved numerically using MATLAB environment. The model has been established assuming unsteady, laminar, hydro-magnetic, fully developed, plane and axisymmetric flow of a gas bubbles-liquid (Diesel-CNG) suspension in a horizontal circular pipe due to the action of an arbitrary time-varying pressure gradient. A uniform transverse magnetic field is applied normal to the flow direction (see Fig.1). The liquid phase (Diesel) is assumed to be electrically conducting depending on its sulfur content. No electric field is assumed to exist and the hall effect of Magnetic Hydrodynamics (MHDs) is negligible. The governing equations for this study are based on the conservation laws of mass and; momentum of both phases.

Fig. 1. Gas-liquid flow under the influence of a magnetic field.

In this simulation, it is assumed that there is no reaction between Diesel and natural gas. Table 1 properties of Diesel Fuel and CNG.

Table 1 Properties of Diesel fuel and CNG

Parameter	Diesel Fuel	CNG
Density (kg/m^3)(20 ºC)	840	0.72
Kinematic Viscosity (cSt) (20 ºC)	2.97	$7.8*10^{-6}$
LCV (Mj/kg)	43.8	45.8
Octane Number	50	125
Carbon (%, w/w)	86.83	73.3
Hydrogen (%, w/w)	12.72	23.9
Oxygen (%, w/w)	1.19	0.4
Sulphur (%, w/w)	0.25	ppm < 5
Electrical conductivity (s/m)	25	-
Relative permittivity	2.0	-

2. GOVERNING EQUATIONS

To formulate the governing equations for this investigation, the balance laws of mass and linear momentum are considered along with consideration of interfacial and external body forces and mutual friction for both phases. It is assumed that both phases are treated as two interacting continua and densities of the liquid and gas remain constant Attia (2006) and Sheng (1990). Under these assumptions, the governing equations are as follows:

2.1 Conservation of Mass

The transport equation for conservation of mass in pipe flow is given as:

$$\frac{\partial \rho}{\partial t} + \frac{1}{r}\frac{\partial(\rho r u)}{\partial r} = 0 \tag{1}$$

ρ, mass density in (kg/m^3), r, radial distance in (m), u, axial velocity in (m/s). For the case in hand, we need two mass conservation equations, one for each phase, and must include the possibility of change phase at the mass rates (η_1, η_2), respectively. We obtain the following mass-balance equations for gas and liquid.

$$\frac{\partial(\alpha \rho_g)}{\partial t} + \frac{\alpha \rho_g}{r}\frac{\partial(r u_g)}{\partial r} = \eta_1 \tag{2}$$

$$\frac{\partial((1-\alpha)\rho_l)}{\partial t} - \frac{(1-\alpha)\rho_l}{r}\frac{\partial(r u_l)}{\partial r} = \eta_2 \tag{3}$$

$$\eta_1 + \eta_2 = 0 \tag{4}$$

Where α, is the void fraction, ρ_g, gas density in (kg/m^3), ρ_l, liquid density in (kg/m^3), u_g, u_l, axial gas and liquid velocities in (m/s) respectively. The true densities for both phases are assumed constant.

2.2 Conservation of Momentum

The governing momentum equations can be written as axial momentum (-z):

For the liquid phase

$$\rho_l\left(\frac{\partial u_l}{\partial t}\right) = -\frac{\partial p}{\partial z} + \frac{\mu_l}{r}\frac{\partial}{\partial r}\left(r\frac{\partial u_l}{\partial r}\right)$$
$$-\frac{\rho_g \alpha}{(1-\alpha)}F_{fric} + F_{mag} \tag{5.a}$$

For the gas phase

$$\rho_g\left(\frac{\partial u_g}{\partial t}\right) = -\frac{\partial p}{\partial z} + \frac{\mu_g}{r}\frac{\partial}{\partial r}\left(r\frac{\partial u_g}{\partial r}\right) +$$
$$\rho_g F_{fric} \tag{5.b}$$

μ_g, μ_l, gas and liquid dynamic viscosity, F_{mag}, magnetic force, F_{fric}, mutual friction force.

2.3 Mutual Friction Force (F_{fric})

About Modeling after Stoke's law, the friction force Sheng (1990):

$$F_{fric} = N(u_l - u_g) \tag{6}$$

$$N = 2\pi n R_b \frac{\mu_l(2\mu_l + 3\mu_g)}{(\mu_l + \mu_g)} \tag{7}$$

Where N, is the momentum transfer coefficient, R_b the average radius and (n) the number of spherical bubbles per unit volume which is related to the void fraction as follows Sheng (1990):

$$\alpha = \frac{4}{3}\pi n R_b^3 \tag{8}$$

2.4 Magnetic Force Acting on the two-Phase flow (Liquid-Gas) (F_{mag})

In this model, the gas is electrically nonconductive, so that the electromagnetic force acts on the liquid only (this assumption depends on the electric conductivity (σ) for the liquid and gas, which for diesel is equal to (25 s/m) depending on the sulfur content of the fuel (sulfur weight 0.25 %) while for CNG is equal to (5*10^{-5} s/m) at 0 ºC) Wyttl *et al.* (2011). Consider magnetic field intensity (B) as given in Fig.2, the magnetic force (F_{mag}) depends on Maxwell's equations is Sheng (1990):

$$F_{mag} = J \times B \tag{9}$$

And, the current density (J) obeys Ohm's law:
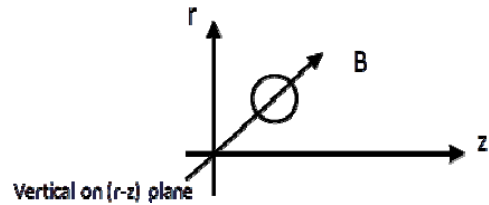
$$J = \sigma(E + u \times B) \tag{10}$$

Fig. 2. Deriving Maxwell's body force.

Where B, is the magnetic field which satisfies Maxwell's equations and σ, is the electrical conductivity of a two phase mixture is expressed by the electrical conductivity (σ_o) of the single phase liquid and the void fraction as follows Sheng (1990):

$$\sigma = \frac{\sigma_o(1-\alpha)}{1 + 0.5\alpha} \tag{11}$$

2.5 Two Phase Flow (Diesel-CNG) in a Horizontal Pipe under a Magnetic Field

Assume that the pressure gradient (- $dp/dz = G$) constant Wyttl *et al.* (2011), $B=Bo$ effect perpendicular on plane (r-z), using Ohm's law equation (10) Attia (2011), and, we derive the equations of the two phase MHD flow in a horizontal pipe from the equations (1) to (5):

$$\rho_l \left(\frac{\partial u_l}{\partial t} \right) = G + \frac{\mu_l}{r} \frac{\partial}{\partial r} \left(r \frac{\partial u_l}{\partial r} \right)$$
$$- \frac{\rho_g \alpha}{(1-\alpha)} N(u_l - u_g) + \sigma(-B_o^2 u_l)$$

(12)

$$\rho_g \left(\frac{\partial u_g}{\partial t} \right) = G + \frac{\mu_g}{r} \frac{\partial}{\partial r} \left(r \frac{\partial u_g}{\partial r} \right)$$
$$+ \rho_g N(u_l - u_g)$$

(13)

Equations (12) and (13) constitute a nonlinear initial-value problem which can be made dimensionless by introducing the following dimensionless variables and parameters:

$$\bar{r} = \frac{r}{R} , \qquad \bar{t} = \frac{t\mu_l}{\rho_l R^2} , \qquad \bar{u}_l(r,t) = \frac{u_l(r,t)\mu_l}{GR^2} ,$$

$$\bar{u}_g(r,t) = \frac{u_g(r,t)\mu_l}{GR^2} , \qquad k = \frac{\rho_g \alpha}{\rho_l(1-\alpha)} , \qquad s = \frac{\rho_g}{\rho_l} ,$$

$$H_a = B_o R \sqrt{\frac{\sigma}{\mu_l}} , \qquad \delta = \frac{\upsilon_g}{\upsilon_l} , \qquad \beta = \frac{NR^2 \rho_l}{\mu_l}$$

By introducing the above dimensionless variables and parameters as well as the expression of the fluid viscosity defined above, Equations (12) and (13) can be written as (the bars are dropped),

$$\frac{\partial \bar{u}_l}{\partial \bar{t}} = 1 + \frac{\partial^2 \bar{u}_l}{\partial \bar{r}^2} + \frac{1}{\bar{r}} \frac{\partial \bar{u}_l}{\partial \bar{r}}$$
$$- k\beta(\bar{u}_l - \bar{u}_g) - H_a^2 \bar{u}_l$$

(14)

$$\frac{\partial \bar{u}_g}{\partial \bar{t}} = \frac{1}{s} + \delta \left(\frac{\partial^2 \bar{u}_g}{\partial \bar{r}^2} + \frac{1}{\bar{r}} \frac{\partial \bar{u}_g}{\partial \bar{r}} \right)$$
$$+ \beta(\bar{u}_l - \bar{u}_g)$$

(15)

The initial boundary conditions of the problem are given as:

$$\bar{u}_l(\bar{r},0) = 0 , \quad \bar{u}_g(\bar{r},0) = 0$$

(16.a)

$$\frac{\partial \bar{u}_l(0,\bar{t})}{\partial \bar{r}} = 0 , \quad \frac{\partial \bar{u}_g(0,\bar{t})}{\partial \bar{r}} = 0 ,$$
$$\bar{u}_l(1,\bar{t}) = 0 , \bar{u}_g(1,\bar{t}) = 0$$

(16.b)

The solutions for $\bar{u}_l$ and $\bar{u}_g$ which satisfy the initial-value problem represented by equations (14) through (16) can be assumed to take the forms

$$\bar{u}_l(\bar{r},\bar{t}) = \sum_{n=1}^{\infty} Pl_n(\bar{t}) \cdot J_o(\lambda_n \bar{r})$$

(17.a)

$$\bar{u}_g(\bar{r},\bar{t}) = \sum_{n=1}^{\infty} Pg_n(\bar{t}) \cdot J_o(\lambda_n \bar{r})$$

(17.b)

Where (λ_n) are the roots of the equation $(J_o(\lambda_n \bar{r})$ (J_o being the zeroth-order Bessel function of the first kind). Substituting Equations (17) and their derivatives into Equations (14) and (15) (with the

non-homogeneous part of these equations represented by a series in $(J_o(\lambda_n \bar{r}))$, and multiplying by $(\bar{r} J_o(\lambda_n \bar{r}))$ Attia (2011) (to take advantage of the orthogonally property of Bessel functions), and then integrating with respect to $(\bar{r})$ from 0 to 1 yields:

$$\dot{Pl}_n + (\lambda_n^2 + k\beta + H_a^2)$$
$$- k\beta Pg_n = a_n$$

(18.a)

$$\dot{Pg}_n + (\delta\lambda_n^2 + \beta)Pg_n$$
$$- k\beta Pl_n = b_n$$

(18.b)

Where a dot denotes ordinary differentiation with respect to $(\bar{t})$ and $(a_n = 2/(\lambda_n J_1(\lambda_n))$ $(J_1(\lambda_n)$ being the first-order Bessel function of the first kind). These equations are combined to give:

$$\ddot{Pl}_n + (\lambda_n^2(1+\delta) + \beta(k+1) + H_a^2)\dot{Pl}_n +$$
$$(\delta\lambda_n^2(\lambda_n^2 + k\beta + H_a^2) + \beta(\lambda_n^2 + H_a^2))Pl_n$$
$$= (a_n + b_n)(\delta\lambda_n^2 + \beta)$$

(19)

The solution of the above linear, ordinary, non-homogeneous, differential equation subject to initial boundary condition Pl_n (0)=0 , Pg_n (0)=0 can be obtained by the usual method of solving such equations to yield

$$Pl_n(\bar{t}) = c_1 e^{\omega_1 \bar{t}} + c_2 e^{\omega_2 \bar{t}} +$$
$$\frac{(a_n + b_n)(\delta\lambda_n^2 + \beta)}{(\delta\lambda_n^2(\lambda_n^2 + \beta k + H_a^2) + \beta(\lambda_n^2 + H_a^2))}$$

(20)

Where ω_1 and ω_2 are the roots of the quadratic auxiliary equation:

$$\omega^2 + (\lambda_n^2(1+\delta) + \beta(k+1) + H_a^2)\omega +$$
$$\delta\lambda_n^2(\lambda_n^2 + k\beta + H_a^2) + \beta(\lambda_n^2 + H_a^2) = 0$$

(21)

And,

$$c_1 = -(a_n + b_n)\left[1 + \frac{\omega_2(\delta\lambda_n^2 + \beta)}{(\delta\lambda_n^2(\lambda_n^2 + \beta k + H_a^2) + \beta(\lambda_n^2 + H_a^2))}\right] /$$
$$(\omega_2 - \omega_1)$$

(22.a)

$$c_2 = (a_n + b_n)\left[1 + \frac{\omega_1(\delta\lambda_n^2 + \beta)}{(\delta\lambda_n^2(\lambda_n^2 + \beta k + H_a^2) + \beta(\lambda_n^2 + H_a^2))}\right] /$$
$$(\omega_2 - \omega_1)$$

(22.b)

The corresponding solution for (Pg_n) can be shown to be:

$$Pg_n(\bar{t}) = \frac{1}{(k\beta)} \left(\begin{array}{l} c_1(\omega_1 + \lambda_n^2 + k\beta + H_a^2)e^{\omega_1 \bar{t}} + \\ c_2(\omega_2 + \lambda_n^2 + \beta k + H_a^2)e^{\omega_2 \bar{t}} + \\ (a_n + b_n)\left(\frac{(\lambda_n^2 + \beta k + H_a^2)(\delta\lambda_n^2 + \beta)}{(\delta\lambda_n^2(\lambda_n^2 + \beta k + H_a^2) + \beta(\lambda_n^2 + H_a^2))} - 1 \right) \end{array} \right)$$

(23)

With the solutions for (Pl_n) and (Pg_n) known, then $(\bar{u}_l)$ and $(\bar{u}_g)$ can be determined from equation (17).

3. RESULTS AND DISCUSSION

3.1 Effect of the Magnetic Field (*Ha*) on (Diesel-CNG) Velocity in a Horizontal Pipe

The solutions reported are numerically evaluated and graphically plotted to various physical parameters on the solutions. Fig. 3 presents the time development of the liquid and gas velocities (u_l, u_g) for various Hartmann numbers (*Ha*) respectively, for various values of *Ha* (0, 1.0, 5.0) and ($r/R = 0$, $\delta = 6.0$, $\beta = 0.5$, $k = 0.01$) at table 2 (A). It is seen in the figures that increasing (*Ha*) decreases the liquid and gas bubbles velocities. The effect of the magnetic field normal to the flow direction imposes rise to a resistive force. Also, it has the tendency to slow down or suppress the movement of the liquid in the pipe (this is consistent with results reported by Malekzadeh *et al.* (2011), Lie *et al.* (1989)). There results demonstrated that the maximum magnitude, of both, global and local velocities was decreased with increasing of the magnetic Bond number, which, in turn reduces the motion of the gas bubbles. This is translated into reductions in the average velocities of both the liquid (Diesel) and bubbles (CNG) phases and, consequently, in their flow rates. In addition, the reduced motion of the gas bubbles in the pipe as a result of increasing the magnetic body force causes lower velocity gradients at the wall. This has the direct effect of increasing the period of transfer of momentum of both of phases.

From Fig. 4, it appears that the slip ratio (u_g / u_l) increased with various magnetic field strengths, it is speculated that the slip ratio increases due to a magnetic ejection effect on bubbles due to the magnetic force resulting from the negative magnetic field gradient. The magnetic ejection effect is an interesting phenomenon where by the non-magnetic material in magnetic fluid is expelled from the region where the magnetic force acts strongly to the region where the magnetic force acts weakly. The results of slip ratio are consistent with results for Malashetty, and Umavathi (1997), and Zaheer *et al.* (2013).

Figure 5 and Figure 6 present the distribution profiles of the liquid (Diesel) and gas bubbles (CNG) velocities, respectively, for various values of Hartmann number (0, 1.0, and 5.0) during different time (0.1, 1.1, 2.1 sec). Figures 5 and 6 show that increasing the parameter (*Ha*) decreases the liquid and gas bubbles velocities for these periods, because of the effect of (*Ha*) on the velocity of the bubbles is more pronounced than its effect on the liquid velocity because it is speculated that the bubbles had been elongating in the direction of the magnetic, the velocity of bubbles are decelerated in the region of positive magnetic field gradient.
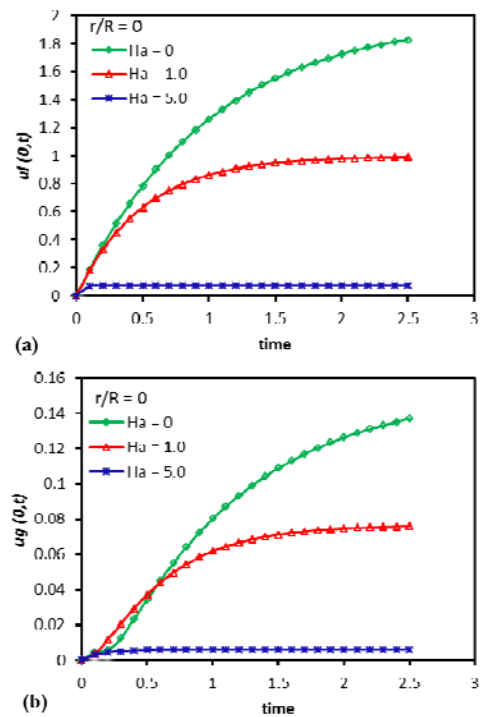

Fig. 3. Time development of (a) liquid; (b) gas velocities for several of Hartmann number (*Ha* = 0, 1.0, 5.0).
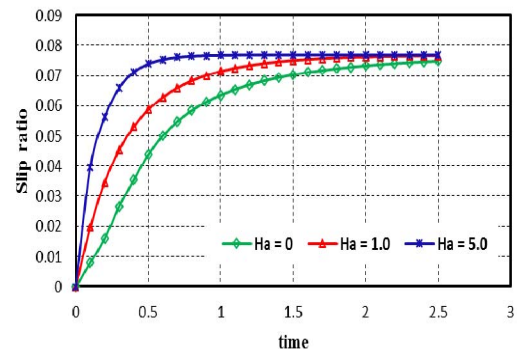

Fig. 4. Slip ratio as a function for time with various magnetic field strengths.

3.2 Effect of Magnetic Field (Ha) on the Momentum Transfer Coefficient (Bubble Size)

The effect of various inverse Stoke's number (β) with increasing the Hartmann number were studied for ranges (0.5, 1.1, and 1.6) at table 2 (B,C), Fig. 7 shows the velocity distribution of the gas bubbles at ($t = 1.1$ sec). The results show that the velocity decreases with increasing both the inverse Stoke's number (β) and Hartmann number. This behavior helped the gas bubbles to change-shapes in the flow under the effect of the magnetic field. On the other hand, the probability of a decrease in bubble radius and an increase of the bubbles number increases with increasing the inverse Stoke's number for the same Hartman number range which in turn contributes to the change for a void fraction. Fig. 8 shows the probability of bubble radius and number

of bubbles. The decrease in gas bubble radius and increase slip ratio in a strong magnetic field due to the magnetic body force. The results for CNG's bubble were agreement for the experimental results of Ishimoto *et al.* (1995).

increased the slip ratio, while increasing both of the inverse Stoke's number (β) and the magnetic field parameter (Ha) increased the probability of decreasing bubble radius and increasing bubble number ($n.R_b$).
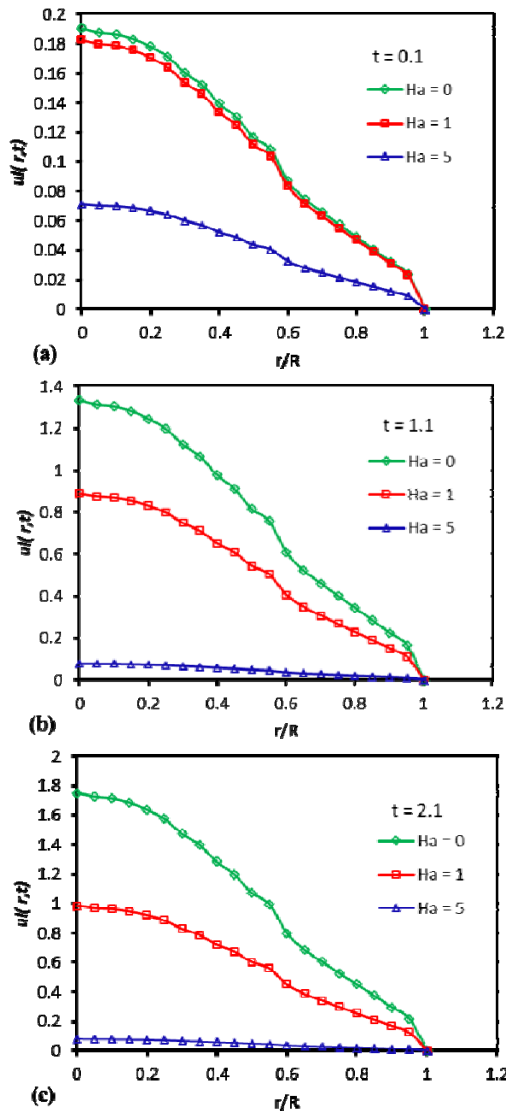

Fig. 5. Velocity distribution of the liquid (Diesel) for several of Hartmann number (Ha = 0, 1.0, 5.0) at time (a) 0.1 sec, (b) 1.1 sec, (c) 2.1 sec.

Fig. 6. Velocity distribution of the gas bubbles (CNG) for several of Hartmann number (Ha = 0, 1.0, 5.0) at time (a) 0.1 sec, (b) 1.1 sec, (c) 2.1 sec.

4. CONCLUSION

The transient MHD flow of a two phase Diesel-CNG in an electrically conducting flow in a circular pipe was studied with consideration of the momentum transfer effects. The governing nonlinear partial differential equations were solved numerically using a Fourier–Bessel series. The effect of the magnetic field parameter (Ha) and momentum transfer coefficient (N) of bubbly Diesel-CNG flow on the transient behavior of the liquid and gas velocities and the probability of changing bubble radius (CNG bubbles) was studied. It was shown that increasing the magnetic field intensity decreased the liquid and gas velocities and
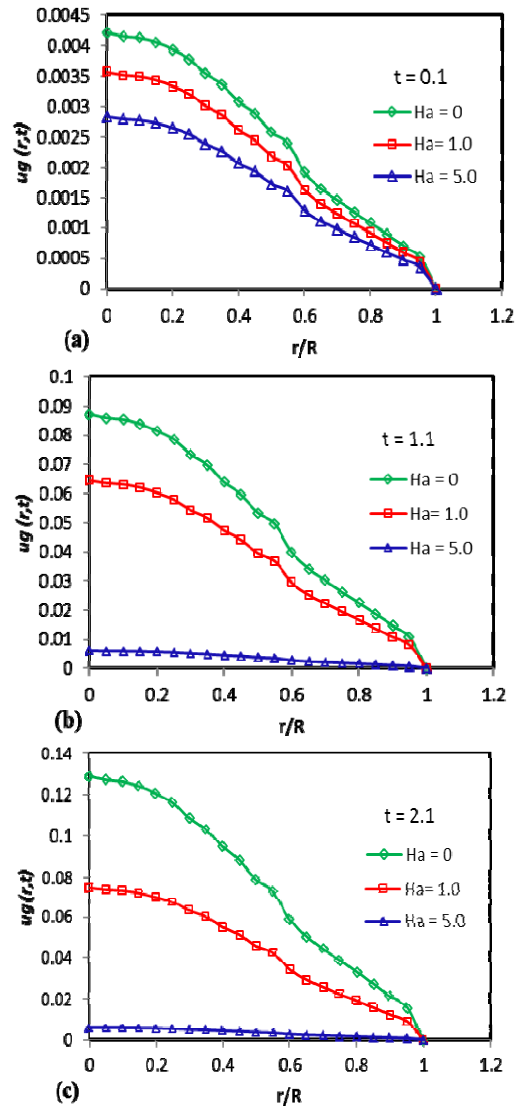

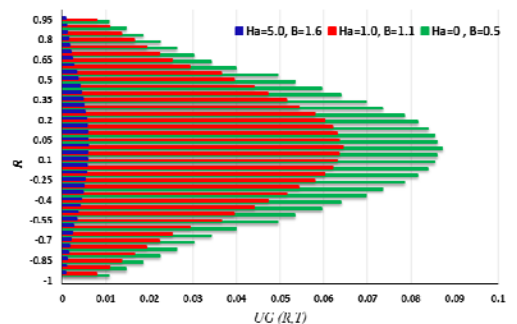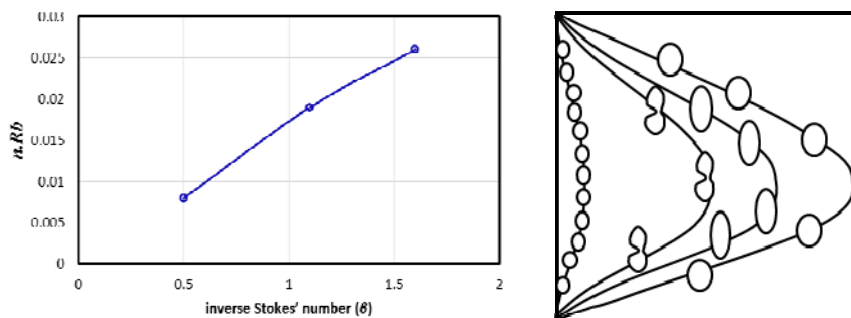**Fig. 7. Velocity distribution of the gas bubbles (CNG) for several of Hartmann number (Ha = 0, 1.0, 5.0) and (β = 0.5, 1.1, 1.6) at time (1.1 sec).**

Table 2 Variation of Diesel and CNG velocities

(A): $r/R = 0$, $\delta = 6.0$, $\beta = 0.5$, $k = 0.01$					
$Ha = 0$					
Time (s)	0.1	0.5	1.0	1.5	2.0	2.5
u_l (m/s)	0.1902	0.7860	1.2617	1.5495	1.7238	1.8292
u_g (m/s)	0.0042	0.0344	0.0803	0.1090	0.1264	0.1369
Slip ratio	0.008	0.0438	0.0636	0.0703	0.0733	0.0748
$Ha = 1.0$					
Time (s)	0.1	0.5	1.0	1.5	2.0	2.5
u_l (m/s)	0.18122	0.63149	0.86327	0.94835	0.97958	0.99104
u_g (m/s)	0.0035	0.0370	0.0617	0.0712	0.0747	0.0760
Slip ratio	0.0196	0.0587	0.0715	0.0751	0.0762	0.0766
$Ha = 5.0$					
Time (s)	0.1	0.5	1.0	1.5	2.0	2.5
u_l (m/s)	0.0711	0.0769	0.0769	0.0769	0.0769	0.0769
u_g (m/s)	0.00282	0.00568	0.00590	0.00591	0.00591	0.00591
Slip ratio	0.0397	0.0739	0.0768	0.07691	0.0769	0.0769

(B): $t = 1.1$ sec, $\delta = 6.0$, $\beta = 1.1$, $k = 0.01$					
$Ha = 0$					
r/R	0	0.2	0.4	0.6	0.8	1.0
u_l (m/s)	1.3314	1.24406	0.97512	0.60805	0.34177	0
u_g (m/s)	0.0872	0.08151	0.06389	0.03984	0.02239	0
$Ha = 1.0$					
r/R	0	0.2	0.4	0.6	0.8	1.0
u_l (m/s)	0.8876	0.8294	0.6501	0.4054	0.2278	0
u_g (m/s)	0.0644	0.0602	0.0472	0.0294	0.0165	0
$Ha = 5.0$					
r/R	0	0.2	0.4	0.6	0.8	1.0
u_l (m/s)	0.07691	0.07186	0.05632	0.03512	0.01974	0
u_g (m/s)	0.0059	0.0058	0.0043	0.00269	0.00151	0

(C): $t = 1.1$ sec, $\delta = 6.0$, $\beta = 1.6$, $k = 0.01$					
$Ha = 0$					
r/R	0	0.2	0.4	0.6	0.8	1.0
u_l (m/s)	1.1114	1.02406	0.8752	0.46605	0.10177	0
u_g (m/s)	0.0673	0.06051	0.05449	0.02998	0.01038	0
$Ha = 1.0$					
r/R	0	0.2	0.4	0.6	0.8	1.0
u_l (m/s)	0.67673	0.60231	0.45112	0.2608	0.18971	0
u_g (m/s)	0.04881	0.04851	0.03881	0.01941	0.00878	0
$Ha = 5.0$					
r/R	0	0.2	0.4	0.6	0.8	1.0
u_l (m/s)	0.03671	0.03291	0.02787	0.01234	0.01017	0
u_g (m/s)	0.00331	0.00312	0.00311	0.00189	0.00101	0

Fig. 8. Probability of ($n.R_b$) with increase the friction parameter.

REFERENCES

Abdul Wahhab, H. A., A. R. A. Aziz, H. H. Al-Kayiem and M. S. Nasif (2015). Modeling of diesel/CNG mixing in a pre-injection chamber. *3rd International Conference Mechanic Engineering Research, IOP Conference Series.* 100.

Attia, H. A. (2003). Unsteady flow of a Dusty Conducting Non-Newtonian Fluid through a Pipe. *Canadian Journal of Physics* 81, 789-795.

Attia, H. A. (2006). Hall Effect on the flow of a dusty Bingham fluid in a circular pipe. Turk. *J. Eng. and Envir. Scin.* 30, 14-21.

Attia, H. A. (2011). Transient circular pipe MHD flow of a dusty fluid considering the Hall Effect. Kragu. *J. Math.* 33, 15-23.

Brunner, K. and J. S. Chang (1980). Flow regime transition under electric fields in horizontal two-phase flow. In *Proceedings 15th IEEE Industry Applications Societal Conference* 1052-1058.

Brunner, K., P. T. Wan and J. S. Chang (1983). Flow pattern maps for horizontal gas liquid two-phase flow under d.c. electric field. In Electrostatics, Inst. *Physics Conference Series* 66, 215-220.

Chamkha, A. J. and S. E. Ahmed (2011). Similarity Solution for Unsteady MHD Flow Near a Stagnation Point of a Three-Dimensional Porous Body with Heat and Mass Transfer, Heat Generation/Absorption and Chemical Reaction. *Journal of Applied Fluid Mechanics* 4(2), 87-94.

Chang, J. S. (1989). Stratified gas-liquid two-phase electro-hydrodynamics in horizontal pipe flow. *IEEE Transitions Industry Applications* 25(2), 241-247.

Chutia, M. and P. N. Deka (2015). Numerical Study on MHD Mixed Convection Flow in a Vertical Insulated Square Duct with Strong Transverse Magnetic Field. *Journal of Applied Fluid Mechanics* 8(3), 473-481.

Gedika E., H. Kurtb, Z. Receblia and A. Keçebaş (2012). Unsteady flow of two-phase fluid in circular pipes under applied external magnetic and electrical fields. *Thermal Sci.* 53, 156-165.

Ghasemi, A., D. J. Olinger and G. Tryggvason (2015, November). Computational simulation of tethered undersea kites for power generation. In *Proceedings of the ASME 2015 International Mechanical Engineering Congress and Exposition, November* 13-19.

Ishimoto, J., M. Okubo, S. Kamiyama and M. Higashitani (1995). Bubble behavior in magnetic fluid under a non-uniform magnetic field. *JMSE International. Journal* 38, 382-387.

Kumar, J. P., J. C. Umavathi and B. M. Biradar (2012). Two-Fluid Mixed Magneto convection Flow in a Vertical Enclosure. *Journal of Applied Fluid Mechanics* 5(3), 11-21.

Kumar, R. and B. G. Prasad (2014). MHD Pulsatile Flow through a Porous Medium. *Journal of Applied Fluid Mechanics* 7(1), 63-74.

Lie, K. H., D. N. Riahi and J. S. Walker (1989). Buoyancy and surface tension driven flows in float zone crystal growth with a strong axial magnetic field. *Int. J. Heat and Mass Tran.* 32, 2409-2420.

Malashetty, M. S. and J. C. Umavathi (1997). Two-phase magneto hydrodynamic flow and heat transfer in an inclined channel. *Int. J. Multi-Phase Flow* 23, 545-560.

Malashetty, M. S., J. C. Umavathi and J. Prathap Kumar (2000). Two fluid Magneto convection flow in an inclined channel. *Int. J. Transport phenomena* 3, 73-84.

Malashetty, M. S., J. C. Umavathi and J. P. Kumar (2001). Convective magneto hydrodynamic two fluid flow and heat transfer in an inclined channel. *Heat and Mass transfer* 37, 259-264.

Malekzadeh, A., A. Heydarinasab and B. Dabir (2011). Magnetic field effect on fluid flow characteristics in a pipe for laminar flow. *Journal Mechanic Science and Technology* 25(2), 333-339.

Mosayebidorcheh, S., M. Hatami, D. D. Ganji, T. Mosayebidorcheh and S. M. Mirmohammadsadeghi (2015). Investigation of Transient MHD Couette flow and Heat Transfer of Dusty Fluid with Temperature-Dependent Properties. *Journal of Applied Fluid Mechanics* 8(4), 921-928.

Raessi, M., J. Mostaghimi and M. Bussmann (2007). Advecting normal vectors: A new method for calculating interface normals and curvatures when modeling two-phase flows. *Journal of Computational Physics* 226(1), 774–797.

Sheng, R. (1990). The effect of magnetic field on two phase liquid metal flow. *Act. Mech. Sci.* 6(2), 128-132.

Wyttl, D., A. Laura, A. Karen and J. Jeffery (2011). Electric properties of polycrystalline methane hydrate. *Geoph. Resc. Lett.* 38(9).

Zaheer, A., H. Jafar and S. Muhammad (2013). MHD two-phase fluid flow and heat transfer with partial slip in an inclined channel. *Therm. Sci.* in press.